Journal of Luminescence 253 (2023) 119462

Contents lists available at ScienceDirect

Journal of Luminescence

journal homepage: www.elsevier.com/locate/jlumin

Full Length Article

Defect-mediated energy transfer in ZnO thin films doped with rare-earth ions

R. Yatskiv [a,*], J. Grym [a], N. Bašinová [a], Š. Kučerová [a,c], J. Vaniš [a], L. Piliai [b], M. Vorokhta [b], J. Veselý [c], J. Maixner [d]

[a] Institute of Photonics and Electronics of the Czech Academy of Sciences, Chaberka 1014/57, Prague, 18251, Czech Republic
[b] Department of Surface and Plasma Science, Faculty of Mathematics and Physics, Charles University, V Holesovickach 2, 180 00, Prague 8, Czech Republic
[c] Faculty of Mathematics and Physics, Charles University, Ke Karlovu 3, 121 16, Praha 2, Czech Republic
[d] Central Laboratories, Institute of Chemical Technology Prague, Technická 5, 166 28, Prague 6, Czech Republic

A B S T R A C T

The rare-earth (RE) (Eu, Er, Nd) doped ZnO thin films were fabricated by a cost-effective chemical solution deposition method. The emission properties of ZnO:RE films were investigated under different excitation conditions, where the RE ions were excited either through direct pumping into the 4f energy levels of RE ions or through indirect excitation by energy transfer from the host material. It is demonstrated that under both excitation methods, the films showed strong emission from the RE ions at room temperature, which confirms the hypothesis that the RE ions can be effectively excited by the host material. Moreover, the influence of RE doping on the development of the crystalline structure of the ZnO thin film was studied. Only a small amount of REs was incorporated into the ZnO grains; most of the REs remained segregated at the grain boundaries, forming a thin oxide shell that strongly suppresses the sintering of the grains and reduces their size.

1. Introduction

Zinc oxide is a promising material for a plethora of applications, including transparent electrodes, thin-film transistors, light-emitting diodes, ultraviolet laser diodes and photodetectors, gas sensors, and piezoelectric nanogenerators [1–6]. The application of ZnO in real devices requires a deeper understanding and control of the optical and electrical properties. A fundamental way to modify the properties of ZnO is the incorporation of dopants. The emission properties of ZnO can be tailored by doping with rare-earth elements to allow for radiative transitions across a wide spectral range from UV to far IR part of the spectrum, which opens opportunities for the application in a variety of optoelectronic devices. The wide-bandgap semiconductors, such as ZnO, GaN, and SiC, are attractive host materials for RE ions since the temperature-quenching effect is inversely proportional to the bandgap of the host [7]. Consequently, a highly efficient luminescence from REs can be achieved. Moreover, it has been demonstrated that RE-doped ZnO has a high potential in spintronics as a diluted magnetic semiconductor with a Curie temperature above room temperature [8].

Indirect excitation by energy transfer (ET) from the host material to REs has attracted attention in recent years since it provides several channels through which the RE ions can be effectively excited. In the case of indirect excitation, there are three processes leading to the RE emission; absorption of excitation energy by the ZnO host, energy transfer from ZnO to the Er ions, and radiative relaxation in the Er ions. The direct energy transfer from the ZnO to RE ions is physically impossible because of the much faster radiative and nonradiative decay of exciton in ZnO than the time required for energy transfer [9,10]. However, RE ions can absorb energy transferred from the DLE of the ZnO host. A few research groups reported indirect excitation of RE ions through a defect level of ZnO [11–18]. However, under indirect excitation in the UV-VIS region, the emission from the host material dominates, and only low-intensity emission from the REs transition was observed. Despite a large number of papers on this topic, the reason why the emission from ZnO:RE thin films is so weak has not been clarified yet. Therefore, one of the important scientific tasks is to understand the optical behavior of RE elements in the ZnO host, which would open the door for enhancing the energy transfer from the semiconductor host to RE ions.

In this work, we investigated the effect of RE doping on the structural, optical, and electrical properties of the ZnO films with an emphasis on the study of indirect excitation of REs by energy transfer from the host material. All selected REs have appropriate energy levels, which can be indirectly excited by the broad defect emission band of ZnO. The presence of RE-related emission under indirect excitation confirms the effective energy transfer between the RE ions and the host

* Corresponding author.
E-mail address: yatskiv@ufe.cz (R. Yatskiv).

https://doi.org/10.1016/j.jlumin.2022.119462
Received 18 March 2022; Received in revised form 3 October 2022; Accepted 25 October 2022
Available online 28 October 2022

material. The emission from REs can be partly affected by the crystallinity of the host crystal. Therefore, this work attempts to shed light on how the mechanism of formation of ZnO:RE thin film influences its optoelectrical properties.

2. Experimental

The zinc oxide thin films doped with different RE ions, erbium, europium, and neodymium, were prepared by the sol-gel method. The initial chemicals were zinc and rare earth species in the form of acetates (Merck) dissolved in 2-methoxyethanol with the addition of monoethanolamine (Carl Roth). The 0.75 M solution of zinc acetate was mixed with 0.1, 1, 2.5, and 5 mol. % addition of the rare earth acetate. The films were deposited by five dip-coating cycles with subsequent annealing of each layer at 350 °C. The final heat treatment followed at 600 °C. Both treatments were carried out in the air. A reference undoped ZnO sample was also prepared.

The morphology of the ZnO thin films was examined by scanning electron microscopy (SEM) (Tescan LYRA3 GM, 20 kV), atomic force microscopy (AFM) (JPK NanoWizard Nanooptics with BRUKER TESPA-V2 tips), and transmission electron microscopy TEM (Jeol JEM-2200FS). The lamellas for TEM measurements were prepared by a lift-out method in dual-beam FIB-SEM system Tescan LYRA3 GM.

The phase composition and the texture of the thin films were characterized by X-ray diffraction (XRD). The XRD data were collected with an X'Pert PRO θ-θ powder diffractometer in Bragg-Brentano geometry using Cu Kα radiation (λ = 1.5406 Å, U = 40 kV, I = 30 mA). The data were scanned with an ultrafast detector X'Celerator over the angular range 25–80° (2θ), using the step size 0.026° and a counting time of 236.64 s step^{-1}.

The chemical composition of the layers was probed by X-ray photoelectron spectroscopy (XPS). The XPS measurements were performed on a custom-built spectrometer (SPECS GmbH) consisting of a hemispherical electron energy analyzer with a 1-D line detector (Phoibos 150 1D-DLD) and a monochromatized Al Kα X-ray source (μ-FOCUS 600 equipped with XR 50 MF) of high intensity. The fitting of the obtained spectra was performed using KolXPD fitting software.

The photoluminescence (PL) spectra were measured using an optical set-up consisting of the Jobin Yvon THR 1000 grating monochromator, a GaAs photomultiplier (R943-02, Hamamatsu Photonics KK, Tokyo, Japan), and a closed-cycle He optical cryostat (4–300 K). A He–Cd laser emitting at 325 nm and a 532 nm solid-state laser were used as excitation sources for the PL measurements. Calibrated neutral-density filters were employed to adjust excitation power density.

The electrical properties of the thin films were studied by the measurement of their current-voltage (I–V) characteristics using a Source Measure Unit Keithley 236 or by Ossila Four-Point Probe station.

3. Results and discussion

3.1. Structural and morphological analysis

As was presented in Fig. 1, the XRD pattern for the undoped ZnO thin film is dominated by the (002) reflection, which points to a strong c-axis texture. After doping with REs, the (002) reflection is still dominant; however, its intensity is suppressed at the expense of (100) and (101) reflections, indicating a more random orientation of the ZnO grains. In addition, for the REs doped films, the (002) reflection peak is shifted to a smaller angle. Such behavior can be associated with increasing interplane distance due to the substitution of Zn by REs with larger ionic radii. Indeed, the radius of Zn is 0.74 Å, while for the REs it is 0.947, 0.88, and 1.013 Å for Eu, Er, and Nd, respectively. At the same time, the average grain size decreased after RE doping (Fig. 2). The lattice strain related to the difference in ionic radii of Zn and REs probably limits the crystallization process [19]. The grain size reduction can be also related to the segregation of RE oxides at the grain boundaries, which

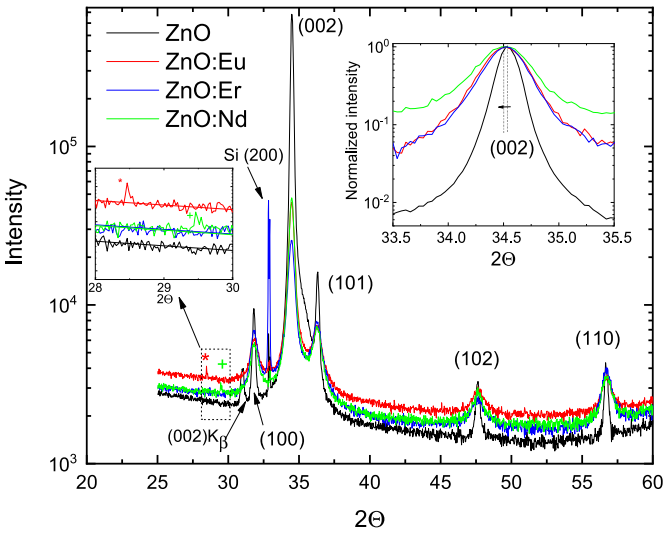

Fig. 1. X-ray diffraction pattern of undoped and RE-doped (2.5%) ZnO thin film prepared by the sol-gel method. Besides the (100), (002), (101), (102), and (110) peaks corresponding to ZnO, the silicon substrate peaks and the (002) K_β reflection are visible in the patterns. The inset represents the shift of (002) reflection due to increasing interplane distance, when REs substitute Zn, due to the large difference in ionic radii. The weak peaks at 2Θ = 28.4° (*) and 29.5° (+) can be associated with the presence of Eu_2O_3 and Nd_2O_3, respectively.

suppresses the coalescence of the ZnO grains. Indeed, as presented in the cross-sectional TEM images (Fig. S1), the undoped film after annealing at 600 °C contains one or two layers of close-packed c-axis oriented polycrystalline grains. In contrast, the ZnO films doped with REs comprise smaller close-packed grains stacked in five layers, which confirms the hypothesis of the presence of a thin RE oxide layer on the surface of the grains that act as stopping barriers for coalescence. The presence of REs oxides is also supported by XRD; the weak peaks at 2Θ = 28.4° and 29.5° can be associated with the presence of Eu_2O_3 and Nd_2O_3 at the grain boundaries. The average crystallite size was extracted from XRD data using the Scherrer formula(not to confuse it with the grain size observed by SEM and AFM). The crystallite size for REs doped samples varied from 10 to 14 nm, while for the undoped samples it is about 58 nm.

3.2. XPS analysis

The undoped and RE-doped ZnO thin films (doped with 2.5% rare earth acetate) were further analyzed by the XPS technique. The XPS survey spectra and high-resolution C 1s, Zn 2p, and O 1s spectra acquired from the undoped and RE-doped ZnO layers are presented in Figs. S2 and S3. The high-resolution Eu 3d, Er 4d, and Nd 3d spectra are shown in Fig. 3. The following information was obtained from the processing and analysis of the spectra in Fig. 3: The high-resolution Eu 3d spectra shown in Fig. 3a can be fitted using two Eu $3d_{3/2}$-$3d_{5/2}$ spin-orbit-split doublets. The doublet at 1134.9–1164.5 eV corresponds to Eu^{3+} trivalent ion, while the doublet at 1125.4–1155 eV corresponds to Eu^{2+} divalent ion [20]. A minor feature at BE of about 1143.6 eV is the shake-up satellite related to Eu^{3+} [21,22]. It should be noted that Eu^{3+} ions were unstable under X-ray irradiation and continuously converted to Eu^{2+} during the XPS measurement (Fig. 3d). In the first spectrum scan, the concentration of Eu^{2+} was almost invisible in the spectrum, indicating that the as-prepared Eu-doped ZnO contains only Eu^{3+}. After 15 scans, its concentration decreased to 40% with respect to the total concentration of Eu. A similar reduction of Eu^{3+} ions to Eu^{2+} was observed for different oxide glasses doped with Eu while irradiating them by γ-rays [23], β-rays [24] or femtosecond laser [25]. It was explained by the fact that the embedded Eu^{3+} ion behaves as an active

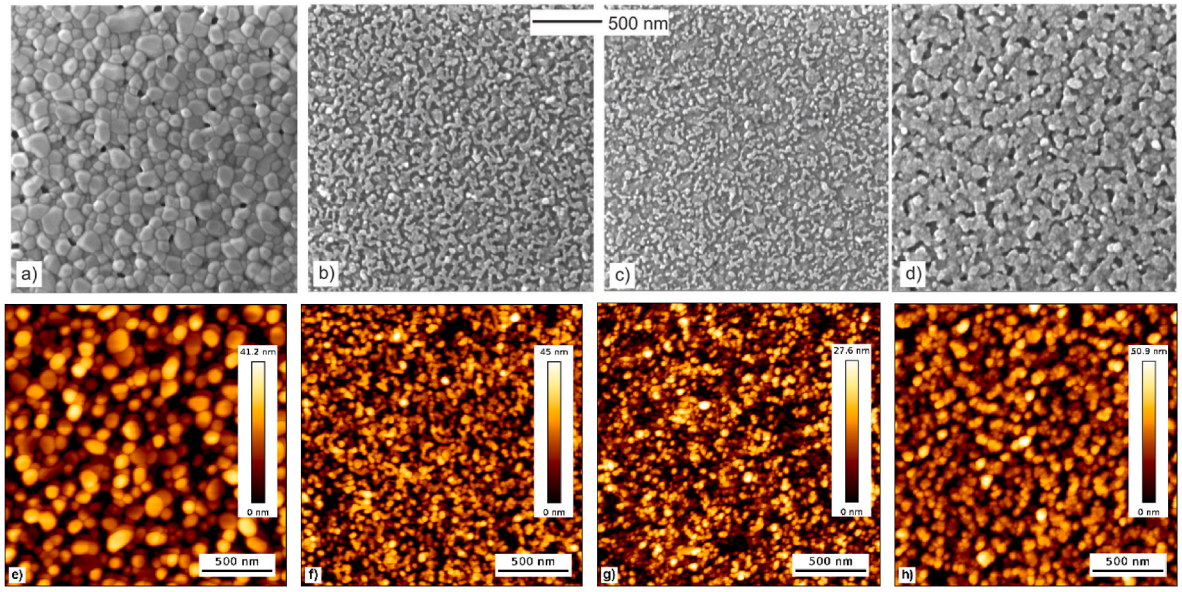

Fig. 2. Top view SEM and AFM images for ZnO thin films prepared by the sol-gel method. (a, e) undoped ZnO; (b, f) ZnO-Eu (2.5%); (c, g) ZnO–Er (2.5%); (d, h) ZnO-Nd (2.5%). The undoped film contains a compact seed layer formed by nanocrystals with an average size of about 58 nm. The average grain size significantly decreased after RE doping, which can be related to the segregation of RE oxides at the grain boundaries, suppressing the coalescence of the ZnO grains and to the strain in the lattice due to the difference in ionic radii for Zn and REs, limiting the crystallization process.

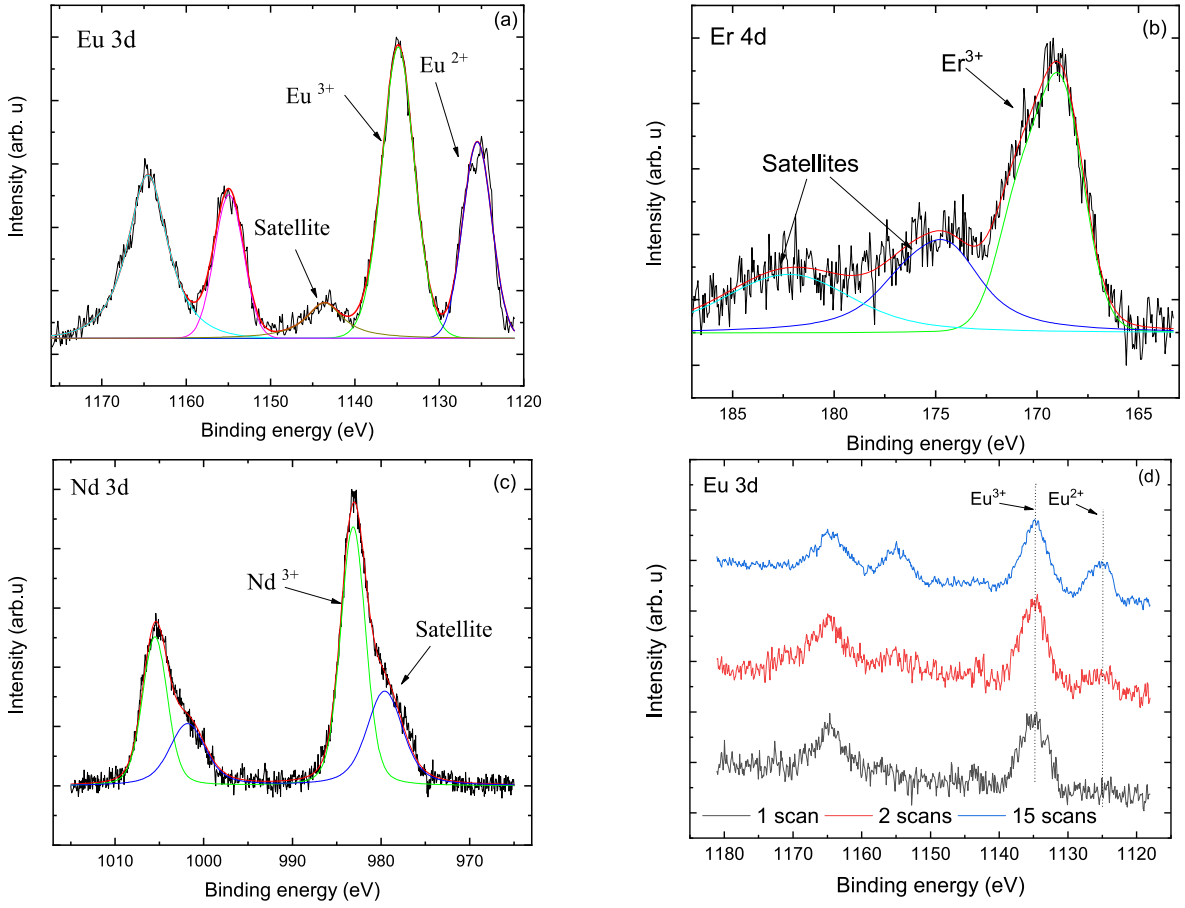

Fig. 3. High-resolution XPS spectra of the ZnO thin film doped with 2.5% RE ions. (a) Eu 3d; (b) Er 4d; (c) Nd 3d. Figure (d) represents the influence of X-ray irradiation on the Eu state in ZnO thin film.

electron trap. If there is a source that creates electrons in the conduction band, some electrons are trapped by the Eu^{3+} ions, leading to the formation of the Eu^{2+} ions. The fact that Eu^{3+} ions were unstable under X-ray irradiation and continuously converted to Eu^{2+} is in accordance with the PL spectra where only red luminescence was observed (it is well known that Eu can be incorporated into ZnO either as Eu^{3+} ions for which red luminescence is dominant or as Eu^{2+} ions with dominant blue luminescence [15]). The high-resolution Er 4d spectra in Fig. 3b exhibited a complex multiplet splitting with the main poorly resolved doublet (the split is about 2 eV) at 168.7 eV accompanied by two satellite features at 174.3 and 181.5 eV. This is a typical spectrum for Er ions in an Er-doped ZnO film and can be associated with Er^{3+} ions dispersed inside the film [26–28]. Finally, the high-resolution XPS spectra of the Nd 3d core presented in Fig. 3c can be described by two peaks at 983 eV and 1005.3 eV that belong to Nd $3d_{5/2}$ - Nd $3d_{3/2}$ doublet of Nd^{3+} ions in Nd_2O_3 [29]. Each component of this doublet shows a multiplet structure typical for Nd oxides, where there are the low BE components at about 879.5 and 1001.7 eV, assigned to the satellite of the main doublet (in the shake-down process) [29].

3.3. Optical properties

3.3.1. ZnO:Eu^{3+}

When Eu^{3+} is exited directly (direct excitation at 532 nm is in resonance with the $^7F_0$ - $^5D_1$ transition of Eu^{3+} ions), at the first step the electrons transfer from $^5D_1$ state to $^5D_0$ state by a nonradiative process. Then the characteristic red emission line is observed at ~580, 594, 614, 656, and 699 nm due to radiative transition from $^5D_0$ to ^7F_j (j = 0,1,2,3,4) (Fig. 4a and S4). The integral emission intensity for all transitions increases with increasing concentration of Eu^{3+} up to 2.5%, and then at 2.5% it significantly decreases (Fig. S5). The quenching of the emission intensity at the highest europium concentration can be explained by the reduction in the average distance between luminescent centers, which enhances the probability of nonradiative energy transfer between Eu^{3+} ions [30]. The presence of the $^5D_0$ -$^7F_1$ emission indicates that some Eu^{3+} ions occupy a site with inversion symmetry. However, the more intense $^5D_0$ -$^7F_2$ emission compared to $^5D_0$ -$^7F_1$ emission and the presence of forbidden $^5D_0$ -$^7F_0$emission indicate that Eu^{3+} ions are primarily located at a low-symmetry site without an inversion center [31].

Under excitation at 325 nm (indirect excitation of Eu^{3+}ions), typical luminescence spectra for ZnO were measured with the near-band edge (NBE) excitonic emission in the UV region and broad deep-level emission (DLE) in the visible region [32]. Nevertheless, in addition to the luminescence from ZnO, the spectra exhibited a sharp peak at 615 nm (Fig. 4b). This emission line is associated with intra-4f transitions of Eu^{3+} ions due to energy transfer from the host material to Eu ions. However, direct energy transfer from the ZnO to Eu ions is physically impossible because of the much faster radiative and nonradiative decay of exciton in ZnO than the time required for energy transfer. Therefore, Eu^{3+} ions can absorb energy transferred from the DLE of the ZnO host and can resonantly excite the $^5D_0$-$^7F_2$ transition (Fig. S4) [33].

3.3.2. ZnO:Nd^{3+}

The luminescence spectra from ZnO:Nd^{3+} were investigated solely under indirect excitation and showed a similar trend as was observed for the ZnO:Eu^{3+} thin film. Apart from the NBE and DLE emission from ZnO, high-intensity luminescence bands were present in the region of 860–1500 nm (Fig. 5a,b and S6). We assume that Nd^{3+} ions can absorb the energy transferred from the DLE of the ZnO host and can resonantly excite the $^4F_{9/2}$ transitions, which are in resonance with the maximum of the DLE emission (Fig. S6). In addition, the broad DLE can also resonantly excite other transitions of Nd^{3+} ions that are located in this region ($^2H_{11/2}$, $^4F_{7/2}$, $^4S_{3/2}$, $^4F_{5/2}$, and $^2H_{9/2}$). At the first step, the electrons transfer from all resonantly excited states to $^4F_{3/2}$state by a nonradiative process. Then the emission band centered at 902, 1082, and 1354 nm due to radiative transition from $^4F_{3/2}$ to $^4I_{9/2}$, $^4I_{11/2}$, and $^4I_{13/2}$ is observed. The integral emission intensity of the Nd^{3+} transition decreases with the increasing concentration of Nd^{3+} (Fig. S7). The presence of the luminescence quenching at such a low concentration of Nd^{3+}ions (~0.1%) can be explained by the higher solubility of Nd in ZnO. The broad character of the three emission bands of Nd^{3+} ions indicates that the luminescence signal originates mostly from Nd_2O_3 [34] located at the grain boundary rather than from Nd^{3+} incorporated in the ZnO crystallites [35]. However, it cannot be excluded that both, Nd^{3+} at the substitutional position and Nd_2O_3 at grain boundaries, contribute to the luminescence.

3.3.3. ZnO:Er^{3+}

Er acts as an optically active center when surrounded by oxygen (ErO_6), forming a pseudo-octahedral structure with C_{4v} symmetry [36]. When Er replaces Zn in the ZnO matrix, ErO_4 forms, which is not an optically active center. In as-prepared samples, only negligible luminescence from Er ions was observed (Fig. S10). However, the formation of ErO_6 clusters can be achieved by annealing. When the ZnO:Er films were annealed at 600 °C, the ErO_6 clusters formed either in the ZnO matrix or at the grain boundaries. Under direct excitation with 532 nm (Fig. 6a; Fig. S8), three well-pronounced emission bands of Er^{3+} (located at 557, 655, and 1539 nm) attributed to down transitions from excited Er^{3+} levels $^4S_{3/2}$, $^4F_{9/2}$, and $^4I_{13/\ 2}$ to the ground state $^4I_{15/2}$ were identified [37,38]. Moreover, the transition from $^4S_{3/2}$ to $^4I_{13/2}$ was observed at about 862 nm. The most intense luminescence band in the VIS range is due to the $^4S_{3/2}$ -$^4I_{13/2}$ transition at 557 nm and in the NIR range due to the $^4I_{13/2}$-$^4I_{15/2}$ transition at 1539 nm. Under indirect excitation with 325 nm the NBE and DLE emissions from the host material were observed in the UV-VIS region (Fig- 6b; Fig. S8). However, also a sharp peak at ~650 nm due to the $^4F_{9/2}$-$^4I_{15/2}$ transition was superimposed onto the broad DLE band. In the NIR region, the transition at ~1530 nm was dominant due to the $^4I_{13/2}$-$^4I_{15/2}$ transition. The presence of two Er-related emission peaks under indirect excitation

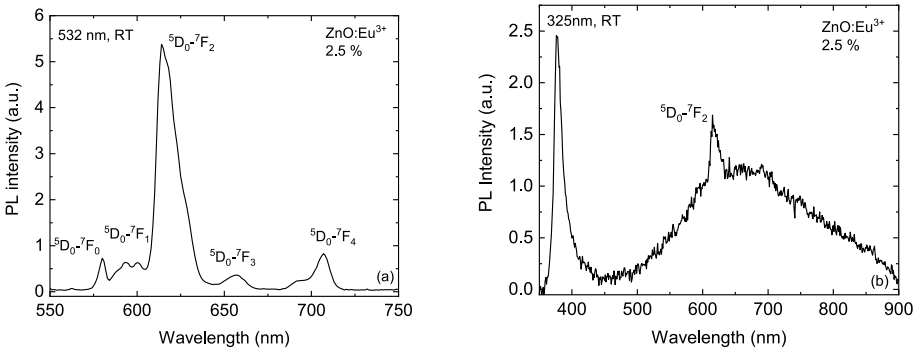

Fig. 4. Room temperature photoluminescence emission spectra for ZnO:Eu thin films under direct (a) and indirect (b) excitation.

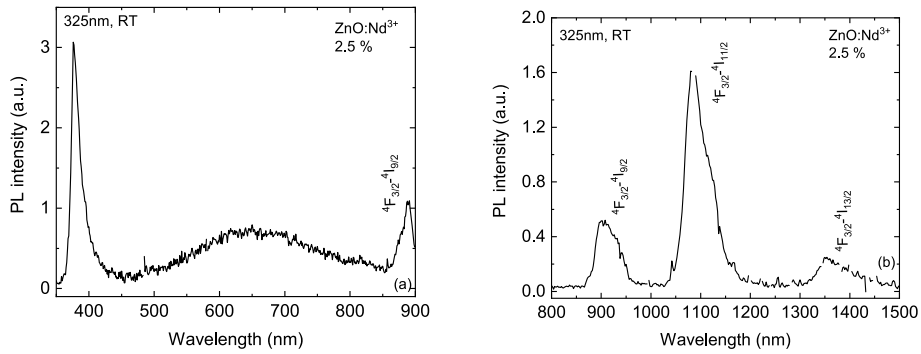

Fig. 5. Room temperature photoluminescence emission spectra for ZnO:Nd thin films under indirect excitation are shown in the spectral range 350–900 nm (a) and 800–1500 nm (b).

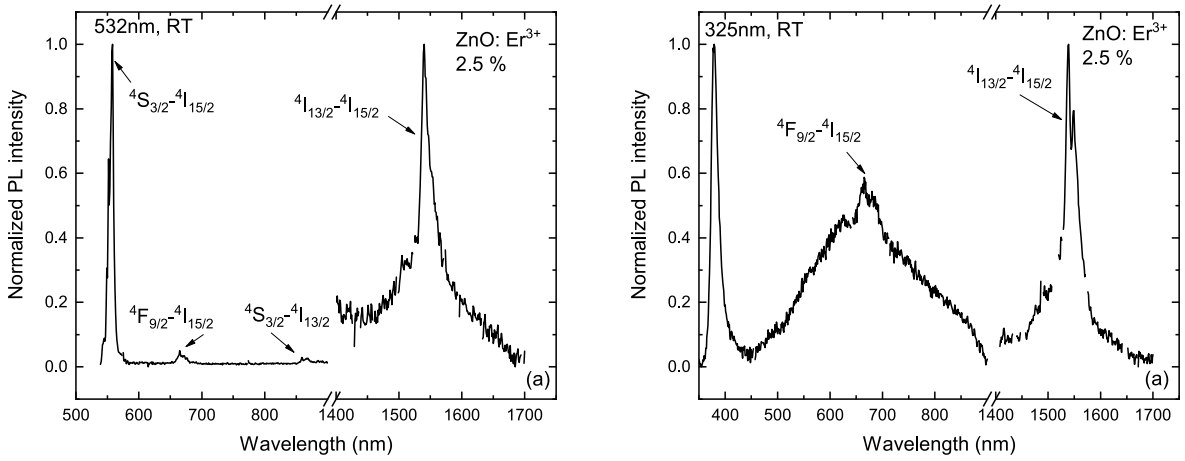

Fig. 6. Room temperature normalized photoluminescence emission spectra for the ZnO:Er thin films under direct (a) and indirect (b) excitation.

confirms the assumption that Er ions are excited due to the energy transfer from the ZnO host. The integral emission intensity of the Er^{3+} transition increases with increasing concentration of Er^{3+} (Fig. S9), which indicates that even at the highest concentration of Er ions (~5%), the conditions for luminescence quenching are not reached.

3.4. Electrical properties

The electrical resistivity of the undoped ZnO thin film was approximately ~82 Ω cm. The dominant transport mechanism for polycrystalline thin films with low doping levels is the grain boundary scattering caused by the thermionic emission over the potential barrier created by surface states at the grain boundaries [39–41]. The effect of doping with RE ions on the resistivity is summarized in Table 1. The resistivity increased after doping with REs, confirming the hypothesis that RE oxides segregate at the grain boundaries, leading to the formation of a barrier for charge transport.

Table 1
Electrical properties undoped and REs doped ZnO thin film.

	Average resistance[a], Ω	Four-point method
		Resistivity, Ωcm
ZnO	8.5E6	81.5
ZnO: 2.5% Eu	2.6E8	**
ZnO: 2.5% Nd	1.3E9	**
ZnO: 2.5% Er	5.6E7	1272

[a] The resistance was calculated from the slope of the I–V curve (Fig. S11). The I–V measurements were performed at several points over the entire area of the sample. A non-alloyed ohmic contact on the top of the ZnO thin film was created by thermal evaporation of a 100 nm film of Al covered with a 50 nm film of Au to prevent surface oxidation. To eliminate the influence of Si substrate on the electrical properties of ZnO thin films, we isolated Si from ZnO by inserting a 600 nm layer of SiO_2; **Out of the range of Ossila Four-Point Probe System.

3.5. Possible mechanism formation of ZnO thin film

Based on the obtained experimental results, the formation of undoped and RE-doped ZnO films can be explained as follows. The as-deposited sol of $Zn(OAc)_2$ started to crystallize gradually after preheating at 350 °C to form a compact polycrystalline film with an average grain size of approximately 10 nm. Further increase in temperature to 600 °C resulted in the increase of the grain size up to 58 nm (Fig. 7a). The film was still composed of at least two layers of grains with the preferential orientation along the c-axis. For the RE-doped sols, the RE were uniformly dispersed in $Zn(OAc)_2$. Similar to undoped ZnO, the preheating at 350° resulted in the nucleation of ZnO and the formation of a compact polycrystalline film. However, the majority of RE ions were not incorporated in the ZnO host lattice because of the large difference in ionic radii and the strong susceptibility of Zn^{2+} and RE to oxidation. It may result in the diffusion of RE towards the surface of ZnO grains and their oxidation. The presence of RE oxides on the surface of the ZnO grains prevented their coalescence, and the annealing at 600 °C had a negligible effect on the increase of their size (Fig. 7b). The cross-sectional TEM image shows that the film is composed of five polycrystalline layers corresponding to five dip-coating cycles (Fig. S1). This indicates that after annealing at 600 °C, each grain is still covered with a thin RE oxide which impedes coalescence of the grains in both vertical and lateral directions.

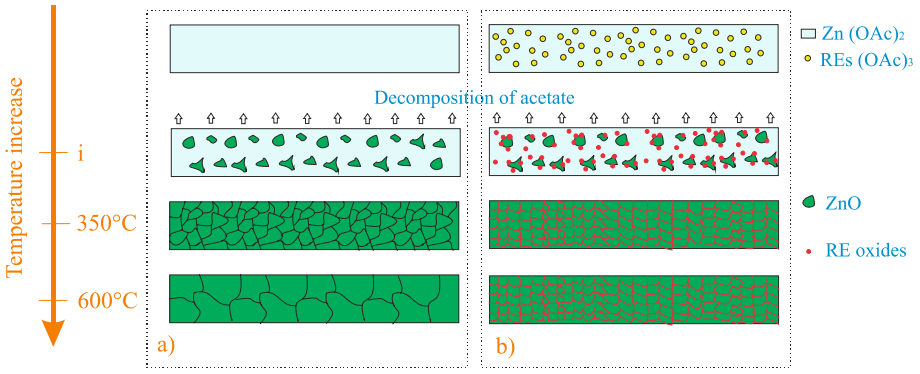

Fig. 7. Formation diagram of the undoped (a) and RE-doped (b) ZnO thin films.

4. Conclusion

The undoped and Eu, Er, Nd-doped ZnO thin nanocrystal films were fabricated by a chemical solution deposition method. After annealing, the undoped films comprised larger crystallites up to 58 nm in diameter and showed a strong c-axis texture. The orientation of RE-doped films was more random and the sintering of the grains was largely suppressed due to the formation of RE oxides at the grain boundaries, which significantly decreased the size of the crystallites. XPS measurements showed that REs were mainly present in its 3+ state; however, Eu^{3+} ions were unstable under X-ray irradiation and continuously converted to Eu^{2+} during the XPS measurement. We assume that the majority of RE ions were not incorporated in the ZnO host lattice; the large difference in ionic radii and the strong susceptibility of Zn^{2+} and RE to oxidation led to the segregation of RE oxides at the grain boundaries. This assumption was supported by the results of optical, electrical, and structural measurements. First, the broad character of the emission bands of RE ions indicated that the luminescence signal mostly originated from RE oxides. Second, the resistivity of the ZnO film increased after REs doping due to the formation of RE oxides at the grain boundaries forming an additional barrier for charge transport. Third, the weak reflections at $2\Theta = 28.4^{\circ}$, and 29.5° in the XRD patterns were associated with the presence of Eu_2O_3 and Nd_2O_3 at the grain boundaries.

We confirmed the possibility of indirect excitation of Eu, Er, and Nd ions through the energy transfer from the host ZnO and showed that both direct and indirect excitations resulted in a highly intensive luminescence at 1.5 μm for ZnO:Er and in the region of 0.86–1.5 μm for ZnO:Nd thin films. This indicates that the energy transfer process is highly efficient. In the visible region, the strong green and red emissions for Er and Eu doped ZnO thin films were observed only under direct excitation since the emission from the host material remains dominant under indirect excitation.

Credit author statement

Conceptualization: RY; writing-original draft preparation: RY, JG and MV; writing – review: RY, JG and MV; thin film preparation: NB; optical characterization: RY; electrical characterization: RY; TEM characterization: SK and JVe; AFM characterization: JVa; XPS characterization: LP and MV; XRD characterization: JM; visualization: RY and MV; project administration: RY; funding acquisition: RY and JG. All authors have read and agreed to the published version of the manuscript

Declaration of competing interest

The authors declare that they have no known competing financial interests or personal relationships that could have appeared to influence the work reported in this paper.

Data availability

Data will be made available on request.

Acknowledgments

This work was supported by the Czech Science Foundation, Project No. 20-24366S, and the Ministry of Education, Youth and Sports of the Czech Republic, project no. 8X20053. L.P. acknowledges the Grant Schemes at Charles University, project registration number CZ.02.2.69/0.0/0.0/19_073/0016935.

Appendix A. Supplementary data

Supplementary data to this article can be found online at https://doi.org/10.1016/j.jlumin.2022.119462.

References

[1] U. Ozgur, Y.I. Alivov, C. Liu, A. Teke, M.A. Reshchikov, S. Dogan, V. Avrutin, S. J. Cho, H. Morkoc, A comprehensive review of ZnO materials and devices, J. Appl. Phys. 98 (4) (2005).
[2] Wang Zhong Lin, Zinc oxide nanostructures: growth, properties and applications, J. Phys. Condens. Matter 16 (25) (2004) R829–R858.
[3] M. Belhaj, C. Dridi, R. Yatskiv, J. Grym, The improvement of UV photodetection based on polymer/ZnO nanorod heterojunctions, Org. Electron. 77 (2020), 105545.
[4] Sheng Xu, Wang Zhong Lin, One-dimensional ZnO nanostructures: solution growth and functional properties, Nano Res. 4 (11) (2011) 1013–1098.
[5] R. Yatskiv, S. Tiagulskyi, J. Grym, J. Vaniš, N. Bašinová, P. Horak, A. Torrisi, G. Ceccio, J. Vacík, M. Vrňata, Optical and electrical characterization of CuO/ZnO heterojunctions, Thin Solid Films 693 (2020), 137656.
[6] L. Piliai, D. Tomeček, M. Hruška, I. Khalakhan, J. Nováková, P. Fitl, R. Yatskiv, J. Grym, M. Vorokhta, I. Matolínová, M. Vrňata, New insights towards high-temperature ethanol-sensing mechanism of ZnO-based chemiresistors, Sensors 20 (2020) 5602.
[7] A.J. Kenyon, Recent developments in rare-earth doped materials for optoelectronics, Prog. Quant. Electron. 26 (2002) 225–284.
[8] K. Potzger, Shengqiang Zhou, F. Eichhorn, M. Helm, W. Skorupa, A. Mücklich, J. Fassbender, T. Herrmannsdörfer, A. Bianchi, Ferromagnetic Gd-implanted ZnO single crystals, J. Appl. Phys. 99 (6) (2006), 063906.
[9] V.V. Travnikov, A. Freiberg, S.F. Savikhin, Surface excitons in ZnO crystals, J. Lumin. 47 (1990) 107–112.
[10] M.Y. Zhong, G.Y. Shan, Y.J. Li, G.R. Wang, Y.C. Liu, Synthesis and luminescence properties of Eu^{3+} - doped ZnO nanocrystals by a hydrothermal process, Mater. Chem. Phys. 106 (2007) 305–309.
[11] D.D. Wang, G.Z. Xing, M. Gao, L.L. Yang, J.H. Yang, T. Wu, Defects-mediated energy transfer in red-light-emitting Eu-doped ZnO nanowire arrays, J. Phys. Chem. C 115 (46) (2011) 22729–22735.
[12] S.M. Ahmed, P. Szymanski, L.M. El-Nadi, M.A. El-Sayed, Energy-transfer efficiency in Eu-doped ZnO thin films: the effects of oxidative annealing on the dynamics and the intermediate defect states, Acs Appl Mater Inter 6 (3) (2014) 1765–1772.
[13] M. Lluscà, J. López-Vidrier, A. Antony, S. Hernández, B. Garrido, J. Bertomeu, Up-conversion effect of Er- and Yb-doped ZnO thin films, Thin Solid Films 562 (2014) 456–461.
[14] Archana Singh, Priyanka Arya, Diksha Choudhary, Surender Kumar, A. K. Srivastava, I.B. Singh, Cost-effective ZnO–Eu3+ films with efficient energy transfer between host and dopant, SN Appl. Sci. 2 (5) (2020) 870.

[15] M. Novotný, M. Vondráček, E. Marešová, P. Fitl, J. Bulíř, P. Pokorný, Š. Havlová, N. Abdellaoui, A. Pereira, P. Hubík, J. More-Chevalier, J. Lančok, Optical and structural properties of ZnO:Eu thin films grown by pulsed laser deposition, Appl. Surf. Sci. 476 (2019) 271–275.
[16] S. Senapati, K.K. Nanda, Red emitting Eu:ZnO nanorods for highly sensitive fluorescence intensity ratio based optical thermometry, J. Mater. Chem. C 5 (5) (2017) 1074–1082.
[17] Samah M. Ahmed, Szymanski Paul, A. Mostafa, El-Sayed, Yehia Badr, Lotfia M. El-Nadi, The photoluminescence properties of undoped & Eu-doped ZnO thin films grown by RF sputtering on sapphire and silicon substrates, Appl. Surf. Sci. 359 (2015) 356–363.
[18] X.Y. Zeng, J.L. Yuan, Z.Y. Wang, L. Zhang, Nanosheet-based microspheres of Eu3+-doped ZnO with efficient energy transfer from ZnO to Eu3+ at room temperature, Adv. Mater. 19 (24) (2007) 4510–4514.
[19] S.-Y. Kuo, W.-C. Chen, F.-I. Lai, C.-P. Cheng, H.-C. Kuo, S.-C. Wang, W.-F. Hsieh, Effects of doping concentration and annealing temperature on properties of highly-oriented Al-doped ZnO films, J. Cryst. Growth 287 (2006) 78–84.
[20] R.M.S. Rayes, Y. Kumar, M.A. Cortes-Jacome, J.A.T. Antonio, X. Mathew, N. R. Mathews, Effect of Eu doping on the physical, photoluminescence, and photocatalytic characteristics of ZnO thin films grown by sol-gel method, Phys. Status Solidi A (2017) 214.
[21] E.-J. Cho, S.J. Oh, S. Imada, S. Suga, T. Suzuki, T. Kasuya, Origin of the high-binding-energy structure in the 3d core-level spectra of divalent Eu compounds, Phys. Rev. B 51 (1995) 10146–10149.
[22] W.-D. Schneider, C. Laubschat, I. Nowik, G. Kaindl, Shake-up excitations and core-hole screening in Eu systems, Phys. Rev. B 24 (1981) 5422–5425.
[23] R. Yokota, Eu^{3+} ion as electron trap in glass, J. Phys. Soc. Jpn. 23 (1967) 129–130.
[24] E. Malchukova, B. Boizot, Reduction of Eu^{3+} to Eu^{2+} in aluminoborosilicate glasses under ionizing radiation Materials Research, Bulletin 45 (2010) 1299–1303.
[25] H. You, M. Nogami, Optical properties and valence change of europium ions in a Sol−Gel Al_2O_3−B_2O_3−SiO_2 glass by femtosecond laser pulses, J. Phys. Chem. B 109 (2005) 13980–13984.
[26] W.-C. Yang, C.-W. Wang, J.-H. He, Y.-C. Chang, J.-C. Wang, L.-J. Chen, H.-Y. Chen, S. Gwo, Facile synthesis of large scale Er-doped ZnO flower-like structures with enhanced 1.54 μm infrared emission, Phys. Status Solidi 205 (2008) 1190–1195.
[27] S. Senapati, K. Kar Nanda, Ultrahigh-sensitive optical temperature sensing based on quasi-thermalized green emissions from Er:ZnO, Phys. Chem. Chem. Phys. 19 (2017) 2346–2352.
[28] G.T.K. Swami, F.E. Stageberg, A.M. Goldman, XPS characterization of erbium sesquioxide and erbium hydroxide, J. Vac. Sci. Technol. 2 (1984) 767–770.
[29] V.V. Atuchin, T.A. Gavrilova, J.C. Grivel, V.G. Kesler, Electronic structure of layered titanate Nd2Ti2O7, Surf. Sci. 602 (2008) 3095–3099.
[30] P.M. Aneesh, M.K. Jayaraj, Red luminescence from hydrothermally synthesized Eu-doped ZnO nanoparticles under visible excitation, Bull. Mater. Sci. 33 (2010) 227–231.
[31] W. Badalawa, H. Matsui, T. Osone, N. Hasuike, H. Harima, H. Tabata, Correlation between structural and luminescent properties of Eu3+-doped ZnO epitaxial layers, J. Appl. Phys. 109 (2011), 053502.
[32] R. Yatskiv, S. Tiagulskyi, J. Grym, O. Cernohorsky, Electrical and optical properties of rectifying ZnO homojunctions fabricated by wet chemistry methods, Phys. Status Solidi A 215 (2018), 1700592.
[33] M.Y. Zhong, G.Y. Shan, Y.J. Li, G.R. Wang, Y.C. Liu, Synthesis and luminescence properties of Eu^{3+} - doped ZnO nanocrystals by a hydrothermal process, Mater. Chem. Phys. 106 (2007) 305–309.
[34] R.B. Yu, K.H. Yu, W. Wei, X.X. Xu, X.M. Qiu, S. Liu, W. Huang, G. Tang, H. Ford, B. Peng, Adv. Mater. 19 (6) (2007) 838.
[35] Yongsheng Liu, Wenqin Luo, Renfu Li, Haomiao Zhu, Xueyuan Chen, Opt Express 17 (12) (2009) 9748.
[36] Masashi Ishii, Shuji Komuro, Takitaro Morikawa, Yoshinobu Aoyagi, Local structure analysis of an optically active center in Er-doped ZnO thin film, J. Appl. Phys. 89 (7) (2001) 3679–3684.
[37] P. Kostka, R. Yatskiv, J. Grym, J. Zavadil, Luminescence, up-conversion and temperature sensing in Er-doped TeO2-PbCl2-WO3 glasses, J. Non-Cryst. Solids 553 (2021), 120287.
[38] J. Zavadil, J. Pedlikova, K. Zdansky, R. Yatskiv, P. Kostka, D. Lezal, Preparation and characterization of telluride glasses, J. Non-Cryst. Solids 354 (2008) 486–491.
[39] Y. Natsume, H. Sakata, Zinc oxide films prepared by sol-gel spin-coating, Thin Solid Films 372 (2000) 30–36.
[40] S. Fay, J. Steinhauser, S. Nicolay, C. Ballif, Polycrystalline ZnO: B grown by LPCVD as TCO for thin film silicon solar cells, Thin Solid Films 518 (2010) 2961–2966.
[41] J.Y.W. Seto, Electrical properties of polycrystalline silicon films, J. Appl. Phys. 46 (1975) 5247–5254.